

Article

Novel Copper Photoredox Catalysts for Polymerization: An In Situ Synthesis of Metal Nanoparticles

Haja Tar ^{1,*}, Tahani I. Kashar ², Noura Kouki ¹, Reema Aldawas ¹, Bernadette Graff ³ and Jacques Lalevée ³

¹ Department of Chemistry, College of Science, Qassim University, King Abdulaziz Rd, Buraydah, Qassim 1162 SA, Saudi Arabia; n.kouki@qu.edu.sa (N.K.); Rdoas@qu.edu.sa (R.A.)

² Department of Chemistry, Faculty of Science, Menoufia University, Shebin El-Kom 32511, Egypt; tahanikashar@yahoo.com

³ Institut de Science des Matériaux de Mulhouse IS2M – UMR CNRS 7361 – UHA, 15, rue Jean Starcky, 68057 Mulhouse CEDEX, France; bernadette.graff@uha.fr (B.G.); jacques.lalevee@uha.fr (J.L.)

* Correspondence: h.tar@qu.edu.sa; Tel.: +966-16-30-13490

Received: 19 September 2020; Accepted: 5 October 2020; Published: 7 October 2020



Abstract: The copper II complex (HLCuCl) carrying 2,4 dinitrophenylhydrazine (L) is synthesized and evaluated as a new photoredox catalyst/photoinitiator in combination with triethylamine (TEA) and iodonium salt (Iod) for the radical polymerization of ethylene glycol diacrylate during exposure to visible light using a photoreactor at 419 nm. The copper complex reactivity with TEA/Iod salt/gold chloride showed a good production and stability of gold nanoparticles. Finally, the high performance of Cu (II) complex for radical photopolymerization incorporating gold nanoparticles is provided. The photochemical mechanisms for the production of initiating radicals are studied using cyclic voltammetry. Polymer nanocomposites containing gold nanoparticles (Au NPs) in situ photogenerated during the irradiation process were prepared. The formation of Au NPs inside the polymer matrix was through UV–Vis and EDS/SEM analyses.

Keywords: copper complex; 2,4 dinitrophenylhydrazine ligand; free radical polymerization; photoredox catalysts; free radical polymerization; gold nanoparticles

1. Introduction

Metal nanoparticle-polymer composites have seen intense research interest in recent years [1–5]. A polymer matrix in which nanoparticles are embedded to enhance some particular properties of the parent matrix is called a polymer nanocomposite. In this method, metal ions are reduced inside a polymer matrix. This technique leads to the homogeneous dispersion of metallic nanoparticles in the polymer matrix [6]. In the past, there has been a lot of work done by different scientists to achieve this specific type of polymer nanocomposite [7–14]. The photochemical synthesis method of gold NPs has attracted a lot of attention because it offers several advantages—for example, convenience, speed, and spatial selectivity. Therefore, the photopolymerization method is widely used for the preparation of nanocomposite materials because it allows the rapid formation of polymer networks with new properties [15]. Nano-coatings are generally prepared by UV irradiation formulations containing dispersed nanoparticles [16]. An in situ photo-polymerization process was used to prepare Ag and Au nanoparticles, as reported in the literature [17–24].

Photopolymerizable formulations generally consist of photoinitiators, oligomers, and additives. Among these constituents, the photoinitiator plays an important role in the final properties of the cured coating, as well as in those of reactive oligomers and diluents. Metal complexes (zinc, ruthenium, iridium, and copper) have been used as photoinitiators for radical and cationic polymerization [25–30].

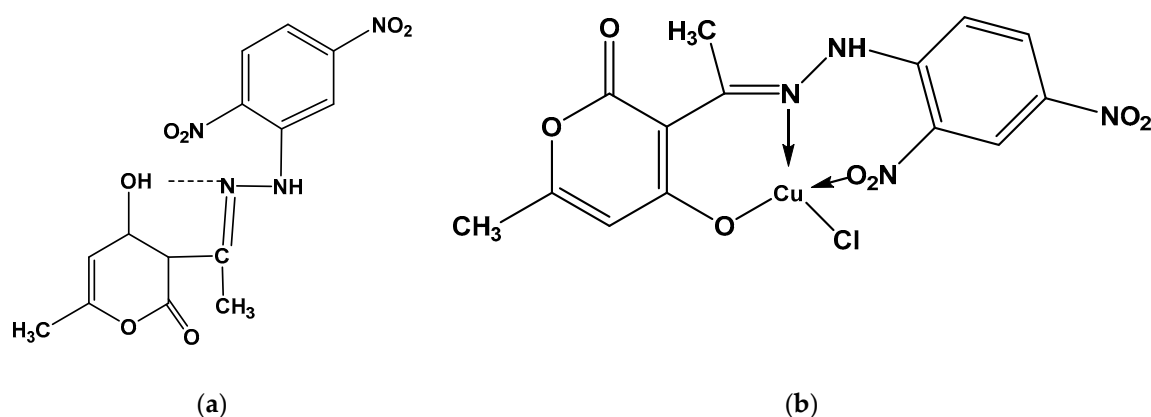
These photoinitiators possess an excellent photochemical property (e.g., the intense absorption of visible light, long-lived excited states, and suitable redox potentials) and can function through an oxidation or reduction cycle to produce reactive species—e.g., radicals, anions, or cations. Recently, copper complexes have been gaining more and more attention in the field of photopolymerization due to their comparative cost advantage. Copper complexes have received increasing attention due to their relative cost, and over the last few years extensive efforts have been devoted to developing copper-based photoinitiating systems (PISs) to initiate photoinitiated polymerization [29–31].

On the one hand, we want to explore the role of new hydrazone ligand in copper II complex used as a photoredox catalyst for polymerization reactions. On the other hand, this later will be tested as a reducer for gold III to gold nanoparticles. Actually, these have attracted scientific interest due to their broad pharmacological profile, including their antitumor, antimicrobial, and antitubercular potential [32–36]. The new copper II complex was incorporated into PIS (containing iodonium salt, triethyl amine, and gold (III) chloride(to generate species (i.e., radicals and cations) and gold nanoparticles inside the polymer matrix. The photoinitiation ability of the copper II complex-based PISs for the radical polymerization and synthesis of networks of interpenetrated gold nanoparticles polymers under light at 419 nm (photoreactor) with an intensity of irradiation of 250 microwatts/cm² will be studied. The reactivity of the system and the photochemical efficiency will be discussed.

2. Materials and Methods

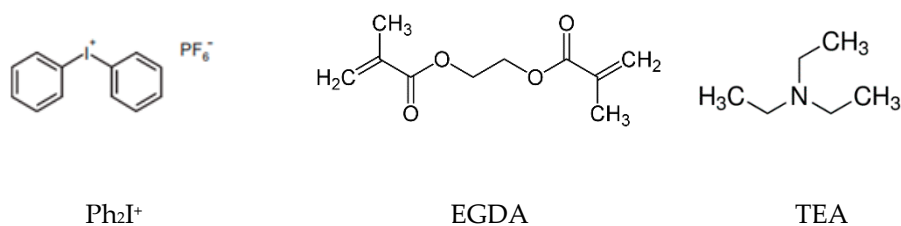
2.1. Materials

The synthesis of this new hydrazone ligand and its copper complex is presented in detail in the supporting information. Remarkably, ligand and its copper complex are completely new (see Scheme 1).



Scheme 1. Structures of the ligand (a) and copper complex (b) used in this study.

Triethylamine (TEA), gold (III) chloride HAuCl_4 , dimethylformamide (DMF), ethylene glycol diacrylate (EGDA), and diphenyliodonium hexafluorophosphate (Ph_2I^+) were obtained from Sigma Aldrich. The following Scheme 2 shows the structure of the chemical compounds used in the photopolymerization processes.



Scheme 2. Chemical structures of the monomers and additives used in this study.

2.2. Irradiation Source

The solution was put into a Pyrex tube (i.d.) 9 mm) and irradiated in a photochemical reactor consisting of a 35 W LED lamp at 419 nm with an irradiation intensity of 250 microwatts/cm² without a water cooling system under an air atmosphere at room temperature.

2.3. Free Radical Photopolymerization

The three-component photoinitiating systems are mainly based on HLCuCl/TEA/Iodonium salt (0.05/1%/1% *w/w*), to the gold (III) chloride added 4wt% in a few drops of DMF, and the PIS system was dissolved in EGDA at 93.95 wt%. The weight percent of the photoinitiating system was calculated from the monomer content. The evolution of the SPR nanoparticles was continuously followed by a Shimadzu UV-1800 spectrophotometer (Shimadzu, Duisburg, Germany). The polymer/composite obtained is characterized by SEM.

2.4. Redox Potentials

The Cu complex oxidation potentials (E_{ox} vs. SCE) were measured in acetonitrile by cyclic voltammetry with tetrabutyl-ammonium hexafluorophosphate 0.1 M as a supporting electrolyte. The free energy change ΔG_{et} for an electron transfer reaction was calculated from the classical Rehm–Weller equation (Equation (1)), where E_{ox} , E_{red} , E^* , and C are the oxidation potential of the electron donor, the reduction potential of the electron acceptor, the excited state energy level, and the coulombic term for the initially formed ion pair, respectively [37]. C is neglected, as is usually in polar solvents.

$$\Delta G_{et} = E_{ox} - E_{red} - E^* + C. \quad (1)$$

2.5. Scanning Image Microscope (SEM)

The morphology and particle size of the polymer was examined by a field emission scanning electron microscope (FESEM) (JEOL JSM 6490-A) at different resolutions.

2.6. Fluorescence Experiments

The fluorescence properties of the copper complex (HLCuCl) were determined in DMF using a JASCO FP-8200 spectrometer (JASCO, Riyadh, Saudi Arabia).

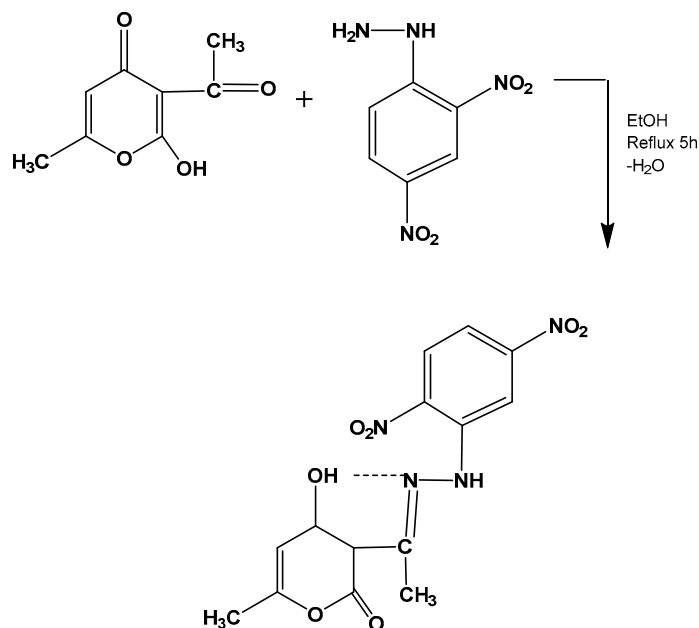
3. Results

3.1. Characterization of the Ligand and Its Copper Complex

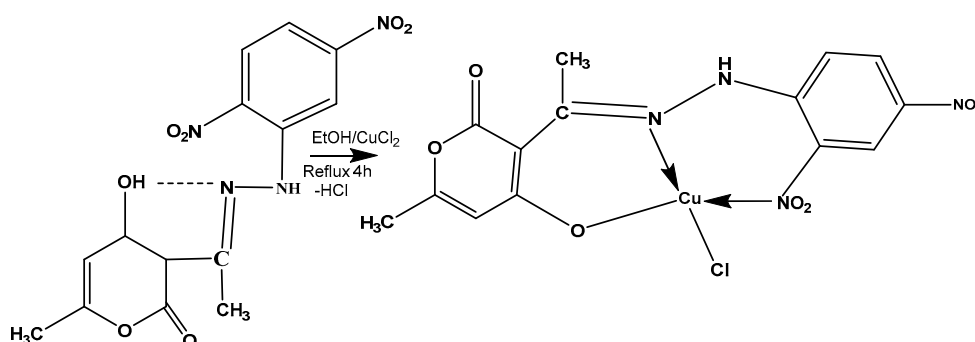
The ligand and the synthesized copper chloride complex were stable at room temperature, freely soluble in DMF, non-hygroscopic in nature, and analyzed on the basis of various spectroscopic techniques to determine their structure. The results of the elemental analysis were in agreement with those of the proposed structure of the synthesized compounds. The observed low conductance values suggested their non-electrolytic nature.

3.1.1. Mass Spectrum

The mass spectrum of the ligand showed an intense molecular ion peak at m/z 348, indicating the formation of a desired compound, as suggested in (Schemes 3 and 4). Other prominent peaks were observed at m/z 313,306,291,267,260, 245,227, 219,198,181,167,151,126,115,109,85,77,67, and 35, respectively (See Figure S1).



Scheme 3. Synthesis of the ligand (HL).



Scheme 4. Synthesis of the complex (HLCuCl).

3.1.2. ¹H NMR Spectrum

The ¹H NMR spectrum of the ligand displayed signals at 2.26 (singlet, 3H) due to $-\text{CH}_3$ proton, 2.45 (singlet, 3H) due to $-\text{N}=\text{C}-\text{CH}_3$, 6.21 (singlet, 1H) due to the olefinic proton of heterocyclic DHA ring, and at 9.0 and 10.9 ppm (singlet, 1H) due to the NH and enolic OH protons, respectively. The very downfield value of enol 1 H NMR indicates a very strong intramolecular hydrogen bonding $\text{O}-\text{H} \cdots \text{N}$. The resonance stabilization of these compounds favours the enol form [38]. The multiple signals appeared at 8.4–7.8 ppm due to an aromatic ring (m, Ar-CH phenyl [39]; Figure S2).

3.1.3. FTIR IR Spectra

The FTIR spectrum of the copper complex was compared with that of the free ligand in order to investigate the mode and nature of the chelation of a metal ion with a ligand. In the FTIR spectrum, the free ligand showed some characteristic bands at 3441, 3098, 2926, and 2852 cm^{-1} , and at 2922, 1716, and 1613 cm^{-1} (see Figure S3) due to OH (intramolecular hydrogen bonding), N–H (stretch), 2C–H (stretch), C=O (carbonyl), and C=N (azomethine) stretching, respectively [40]. In the copper complex, the disappearance of a band centered at 3441 cm^{-1} suggests the deprotonation of enolic proton and the involvement of the enolic oxygen atom in the coordination with the copper ion. Increasing the frequency of the C=N band at 1614 cm^{-1} compared to that of the free ligand indicates the involvement of the azomethine group in coordination with the copper ion [41], suggesting that copper ions coordinate through the oxygen atom and the nitrogen of the atom azomethine group [40]. Moreover, the spectrum

consists of three non-ligand bands at 555, 517, and 449 cm^{-1} which can be assigned to the Cu–O, Cu–N, and Cu–Cl vibrations, respectively [42]. The ligand HL behaved as monobasic tridentate towards cupric ions. The proposed structures of the copper complex are presented in Figure S4.

3.1.4. The DTA and TGA Spectra

The diagram of the ligand is illustrated in Figure S2. The DTA diagram shows an endothermic peak at 132.28 °C with no weight lost, as also indicated by the TGA curve due to the melting of the compound. The exothermic peak appeared at 238.91 °C in the DTA curve and started at 219.92 °C and ended at 300.7 °C in the TGA curve, with a weight loss of 37.77%, and may be assigned to losses of para nitro aniline. Another two peaks appeared at 317.15 and 444.43 °C in the DTA curve and in the TGA curve at 300.73–411 and 411–1001.35 °C, with a weight loss of 16.02% and 25.82%, respectively, and were assigned to the chemical decomposition of organic compound; see Figure S5.

3.2. Light Absorption and Magnetic Properties of Cu-Complex

The calculated UV–Vis absorption (at the UB3LYP/6-31G* method) of the copper complex is plotted. In Figure 1a, this last UV-vis transition is compared with the actual experimental UV–Vis spectra in Figure 1b.

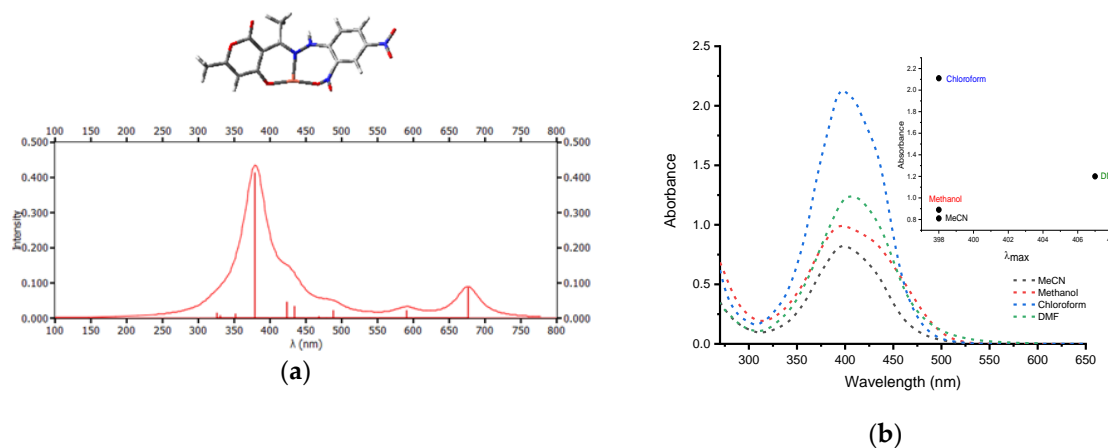


Figure 1. Optimized (by the UB3LYP/6-31G* method) (a) copper complex geometries and their UV–Vis spectra; (b) UV–Visible spectra of HLCuCl complex in MeCN, methanol, and chloroform, and in a DMF concentration of 10^{-4} M.

The UV–Vis. electronic spectra of the copper II complex in four organic solvents with different polarities were also studied. The UV–Vis. absorption spectra of the studied complex were measured in dimethylformamide, ethanol, chloroform, and acetonitrile. Figure 1b shows the absorption spectra of a 10^{-4} mol L $^{-1}$ solution of HLCuCl in these solvents as a sample. As can be seen from Figure 1b, all the solvents tested the main band of the studied compound, which was located in the spectral range of 398–407 nm. This band is characteristic of ligand–metal charge transfer transition (LMCT) [43–45]. In the UV–Visible region observed from the studied compound in different solvent systems, this is assigned to the $\pi \rightarrow \pi^*$ transition of the C=N [46]. The copper II complex is characterized by high molar extinction coefficients in the different solvents (see Table 1).

Table 1. Molar extinction coefficients ϵ in different solvents for the cu-complex investigated.

ϵ ($\text{M}^{-1} \text{cm}^{-1}$)	λ_{max} (nm)	Solvents
8270	398	Acetonitrile
9900	398	Methanol
12,390	407	DMF
21,260	398	Chloroform

The observed band and the magnetic moment 1.72 B.M. of copper (II) complex are close to the spin-only value of one unpaired electron, indicating a square planar geometry around the Cu(II) ion [47] and suggesting a square-planar geometry around the copper ion [48,49].

The HOMO and LUMO calculated from molecular orbital calculations well show this π - π^* transition character (Figure 2) with frontier orbitals well-delocalized on the ligand with a participation of the Cu center.



Figure 2. Contour plots of HOMOs and LUMOs for the copper complex structure optimized at the B3LYP/6-31G* level of theory.

3.3. Copper Complex Oxidation Process

The oxidation potential of E_{ox} from the copper complex is presented in Table 2 in acetonitrile. It was evaluated by measuring the cyclic voltammetry with tetrabutyl-ammonium hexafluorophosphate 0.1 M as a supporting electrolyte. dissolved oxygen was removed by bubbling nitrogen gas (see Figure S6.). The excited state energies were evaluated from the crossing point of the absorption and luminescence spectra (see Figure S7).

Table 2. Excited state energies E^* , oxidation potentials E_{ox} , and free energy change (ΔG_{et}) for the HLCuCl/TEA/Iod interaction.

E_{ox} vs. SCE* [V] [HLCuCl]	E^* [eV] [HLCuCl]	ΔG_{et} (HLCuCl II/Iod) (eV)	ΔG_{et} (HLCuCl II/TEA) (eV)
1.44	2.8	-1.16	-0.82

The free energy change ΔG_{et} for the electron transfer reaction between the copper complex and diphenyliodonium hexafluorophosphate (Iod), TEA, or gold chloride was calculated from the classical Rehm–Weller equation (Equation (1)) [34]. The free energy change of the HLCuCl/Iod electron transfer reaction $\Delta G_{et} = -1.16$ eV is highly negative and make the process favorable (using E_{red} (Iod) = -0.2 eV) [50]. The counteranions of iodonium salts would not affect the results of the photochemical mechanism studies for the initiation process. For the reaction between the copper complex and the triethylamine, it is $\Delta G_{et} = -0.82$ eV, which also supports a favorable electron transfer process (using $E_{ox} = 1.079$ V for the triethylamine) [51].

3.4. Photoinduced Synthesis of Au Nanoparticles

Noble metals are known to exhibit unique optical properties due to their property of Surface Plasmon Resonance (SPR), which is the collective oscillation of the conduction electrons in resonance with the wavelength of the irradiated light. In the present study, the formation of gold nanoparticles was initially conformed using UV–Visible spectroscopy by measuring the SPR peaks. Gold nanoparticles exhibit plasmon absorption bands that depend on their size and shape.

We report the use of triethylamine as reducing agents in the formation of gold nanoparticles in the presence of a copper complex and iodonium salt. The study of Newman et al. [51] indicates the utility of amines as reducing agents in the formation of AuNPs and provides information on the conditions under which these reactions will take place.

For the synthesis of gold nanoparticles, 1 mL of TEA was added to 1 mL of gold chloride and 1 mL of HLCuCl solution in DMF. The sample was stirred continuously for 5 min. at room temperature.

The HLCuCl/TEA/HAuCl₄ system shows the increase in the absorption at 362 nm during irradiation, with the appearance of a peak at 525 nm. The color gradually changed from yellow to dark purple within a minute of irradiation (see Figure 3). The absorption at 525 nm corresponding with the SPR peak and the change in colors and characteristics of the surface plasmon absorption spectra indicates the formation of Au nanoparticles with the size of 30 nm [52,53].

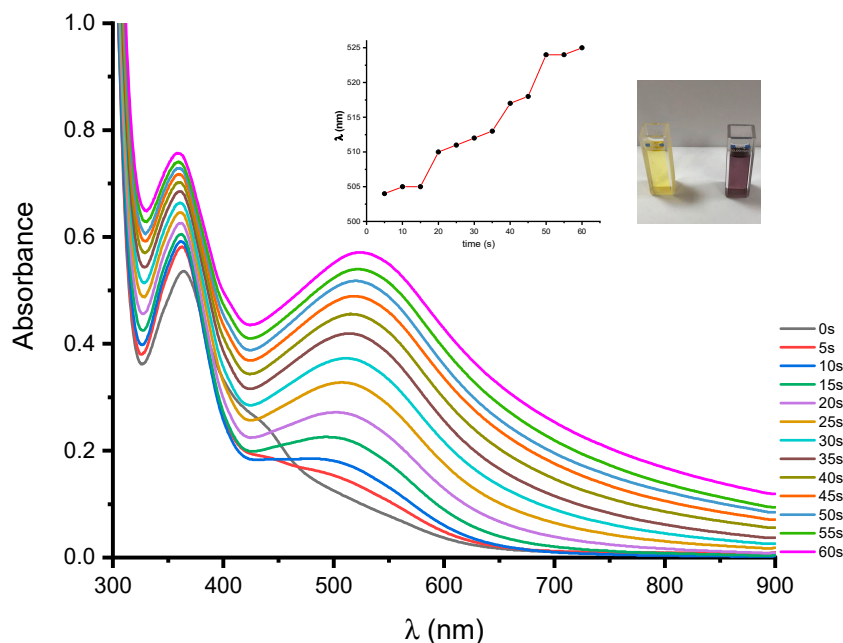


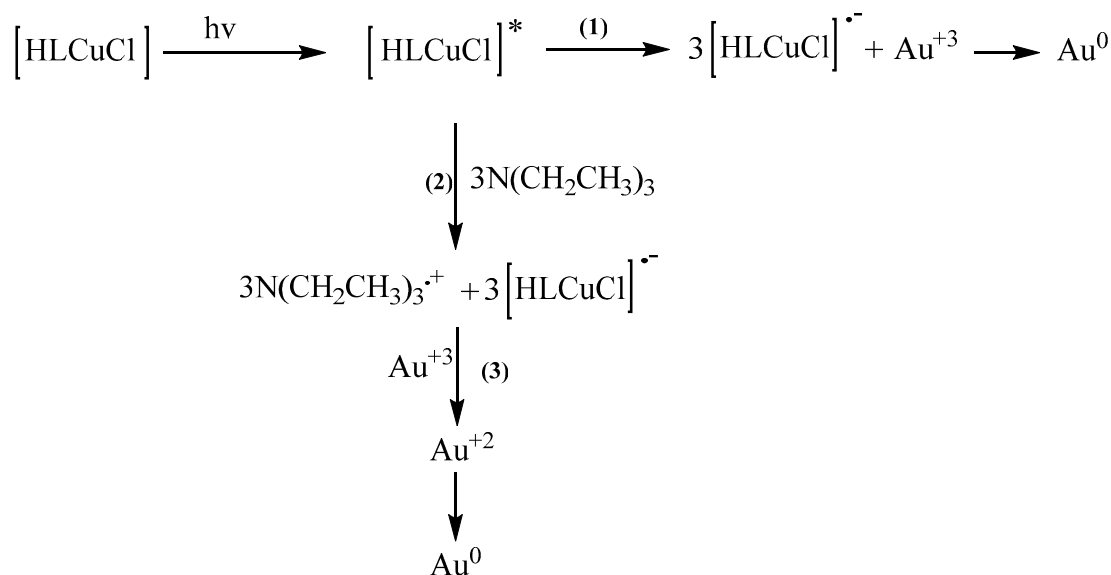
Figure 3. Evolution of the absorption spectra of the irradiated mixtures ($\lambda_{irr} = 419$ nm). Solution: HLCuCl 0.05 wt % gold chloride 4wt% and TEA 1 wt% dissolved in 25 mL of DMF.

The inserts in Figure 3 show the time traces for the maximum position of the plasmon band for the system based on copper complexes and triethylamine; a clear red shift is observed during the initial stages of the process. The interaction of the copper complex, triethylamine, and gold chloride was very fast, being within 60 s. A small amount of copper complex was sufficient to generate radical ions, which reduce the tetrachloroaurate to form Au⁺². This is disproportionate to Au⁺³, which is then reduced to Au⁰, leading to the formation of nanoparticles (see Figure S8). Moreover, the reduction of HAuCl₄ occurs due to a transfer of electrons from the amine to the metal ion, resulting in the formation of Au⁰, with the reaction being generically described according to Scheme 5.

The system which contains copper II complex 0.05 wt% gold (III), chloride 4 wt%, and Iodonium salt 1 wt% dissolved in 25 mL of DMF shows better efficiency in producing gold nanoparticles under visible irradiation at 419 nm, with an intensity of 250 microwatts/cm². Figure 4 shows the appearance of the absorption band of Au⁺³ at 328 nm [54] at t = 0 s, and also the maximum absorption of the HLCuCl complex at 407 nm after one minute of irradiation, where we have seen a large decrease in the band at 328 nm and the change in the color to orange. After five minutes under irradiation, the absorption of the complex and Au⁺³ have entirely disappeared; we notice the increase in absorption at 525 nm, which corresponds the surface plasmon resonance (SPR) absorption. A careful analysis of the absorption spectrum during the irradiation period clearly reveals the following:

- The first step corresponds to the photobleaching of HLCuCl with the concomitant growth of the surface plasmon band, as indicated by the linear correlation between the absorbance at 407 nm vs. the absorbance at 525 nm (inset in Figure 4).
- In a second step, the decomposition of the iodonium salt through an electron transfer and the production of a phenyl radical that is able to abstract hydrogen to generate radicals reduces the Au⁺³ to Au⁺². The Au⁺² is unstable and can be reduced with the radical to Au⁺¹ [12].

Then, the Au^{+1} can be reduced by another radical to Au^0 . Scheme 6 illustrates the proposed reaction mechanism.



Scheme 5. Proposed mechanism of the system based on HLCuCl/TEA.

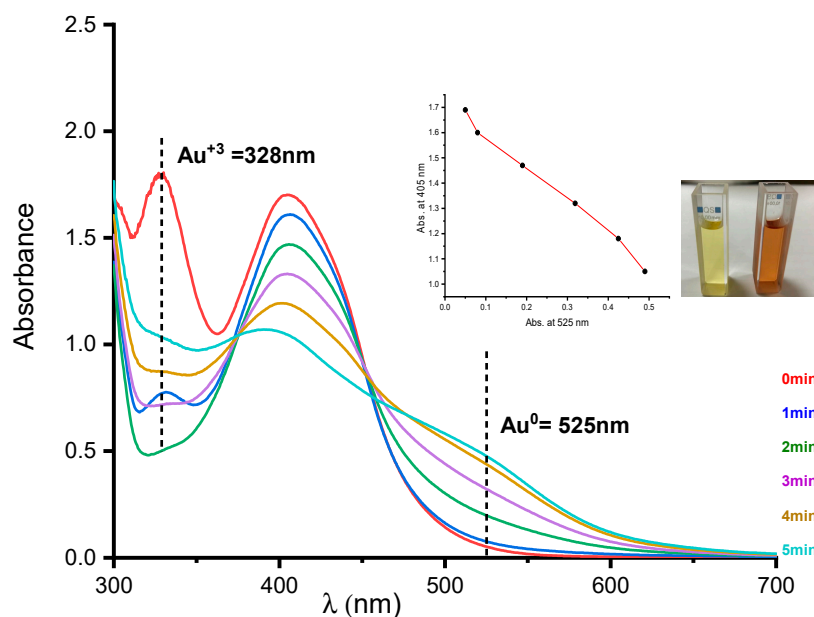
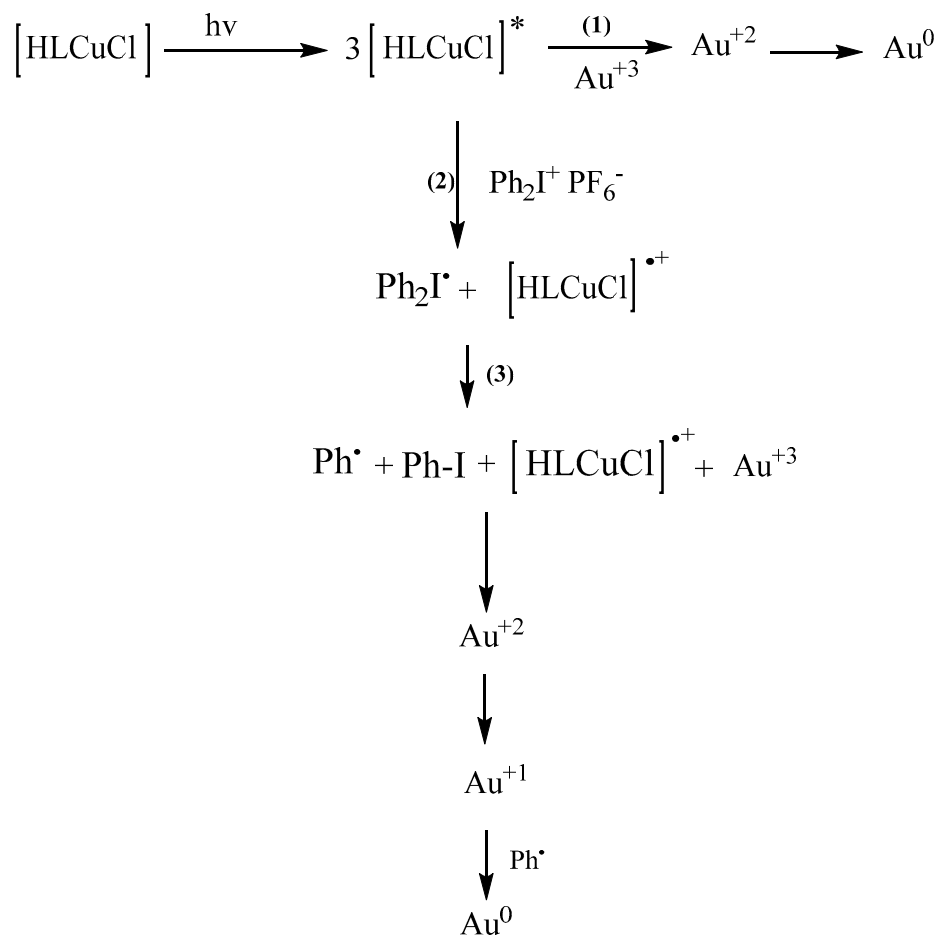


Figure 4. Evolution of the absorption spectra of irradiated mixtures ($\lambda_{\text{irr}} = 419 \text{ nm}$). Solution: HLCuCl 0.05 wt% gold chloride 4wt% and iodonium salt 1 wt% dissolved in 25 mL of DMF.

Figure 5 illustrates the UV–Vis absorption spectra of the PIS system HLCuCl/TEA/Iod solution obtained during irradiation in the presence of gold chloride. The formation of gold nanoparticles in the PIS take places through the reduction of Au^{3+} to Au^0 , and this outcome can be proven by the appearance of characteristic plasmons in the UV–Vis absorption spectra at 536 nm. The peak has a symmetrical shape, indicating the uniform size distribution of the gold nanoparticles in the organic phase [55]. The insert in Figure 5 shows that the SPR band changes with the irradiation time, and it was also noticed that the violet color grew increasingly darker with the radiation time. These results show that a simple irradiation of a copper complex in the presence of HAuCl_4 leads to its reduction, with the rapid generation of both metallic gold and initiating radicals without any undesirable side reactions.



Scheme 6. Proposal mechanism of the system based on HLCuCl/Iod salt.

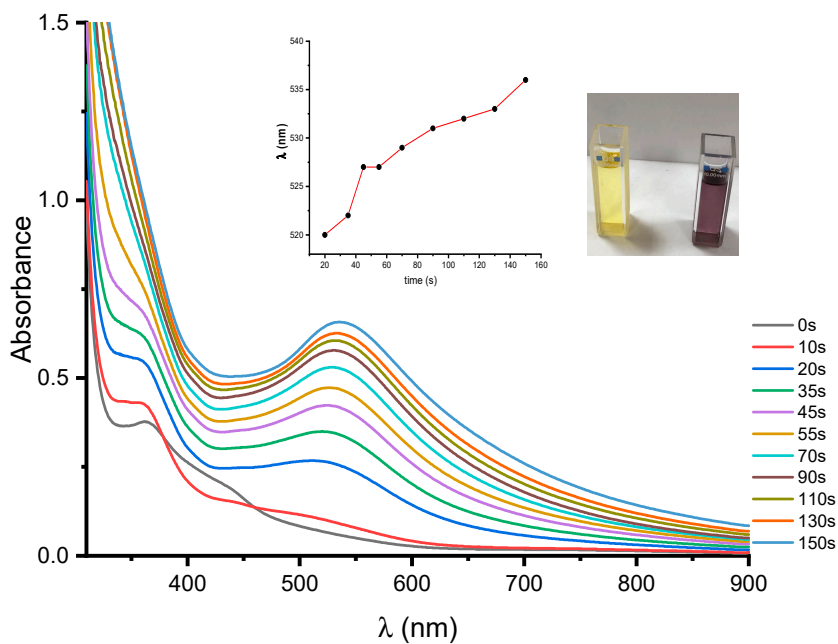


Figure 5. Evolution of the absorption spectra of irradiated mixtures ($\lambda_{\text{irr}} = 419 \text{ nm}$). Solution: HLCuCl 0.05 wt% gold chloride 4wt%, TEA 1wt%, and iodonium salt 1 wt% dissolved in 25 mL of DMF.

3.5. Fabrication of AuNPS Embedded Polymer

Metal ions are reduced inside a polymer matrix. This technique leads to a homogeneous dispersion of the metallic nanoparticles in the polymer matrix. The in situ process to prepare and stabilize nanoparticles can be combined in one step. This process gives the opportunity of a quick and easy way to synthesize stabilized NPs.

The UV-crosslinked irradiated for 10 min under air were subjected to UV-Vis spectroscopy analyses. The sample consists of HLCuCl/Iod/TEA as the photoinitiating system in the presence of gold chloride, and EGDA was used as a monomer. The photopolymerization formulation was prepared by HLCuCl 0.05 wt% gold chloride 4 wt% in a few drops of DMF, TEA 1 wt%, and iodonium salt 1 wt% dissolved in EGDA at 93.95 wt%. The last was stirred continuously overnight at room temperature.

The spectra in Figure 6 show a clear and strong absorption band centered at 532 nm and another peak at 407 nm, as had happened for the photoinitiating system solutions HLCuCl/Iod/TEA in the presence of HAuCl₄ in the spectra of Figure 5. The intensity of the band is similar to that seen in the spectra of Figure 6. The strong absorption peak at 532 nm can be attributed to the formation of plasmon resonance gold nanoparticles, as was previously recorded for the UV irradiation of a photoinitiating system containing the gold ion. The peak at 407 nm is related to the HLCuCl. The formation of the narrow SPR band of AuNPs clearly confirms the formation of Au nanoparticles in the cross-linked acrylate formulation by UV irradiation. The color changes of these gels from yellow to dark purple also represent unambiguous proof in favor of the AuNPs development and deposition within the polymeric template. The color changes in these gels range from a transparent color to a purple-colored form depending on the irradiation time.

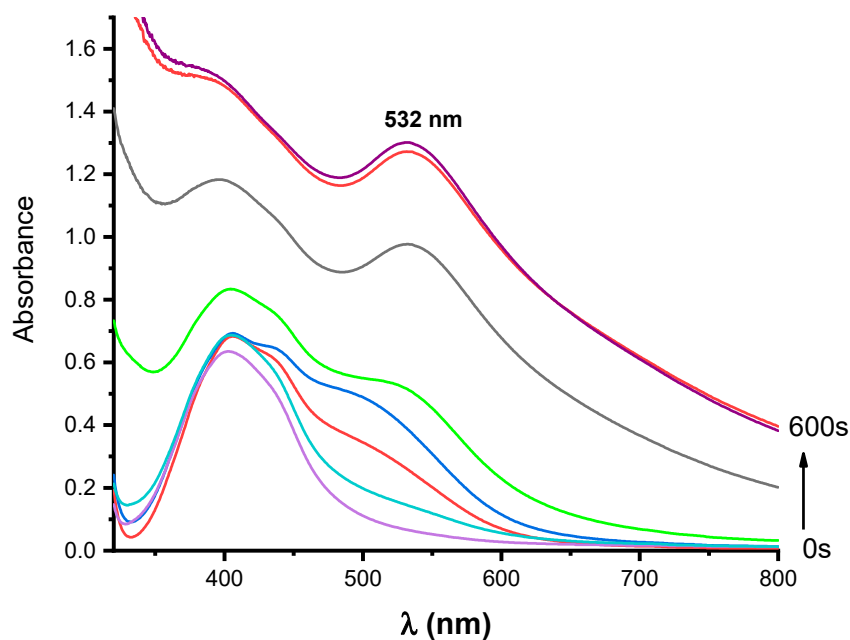


Figure 6. Time evolution of the absorption spectrum of the ethylene glycol diacrylate (EGDA) during photopolymerization, irradiated mixtures ($\lambda_{\text{irr}} = 419 \text{ nm}$). Solution: HLCuCl 0.05 wt% gold chloride 4wt%, TEA 1wt%, and iodonium salt 1 wt% dissolved in 93.95 wt%.

SEM measurement also supported the controlled size distribution of AuNPs without agglomeration; see Figure 7. The increase in the density of the cross-links of the nanocomposite material led to the formation of large-sized AuNPs. The SEM images and SPR absorbance of the AuNPs support this (see Figures 6 and 7). The shape of AuNPs is mainly spherical, and the size is controlled. The size, shape, and distribution of AuNPs were facilitated by HLCuCl, but the ethylene glycol-based acrylic monomer also contributed to this due to the chelation effect [22]. A difference in size is observed with ranges between 37 and 200 nm (see Figure 7). The overall crosslink efficacy

depends on the UV light intensity, the dose (or irradiation time), and the concentration of the initiator and gold chloride. The selected relative concentration of 0.05 wt%, 4 wt%, and 1 wt% have not been optimized. Furthermore, a higher UV light intensity will accelerate the crosslink; however, it might also reduce the efficacy. Greater background may be found in the kinetic models of Lin et al. [56,57].

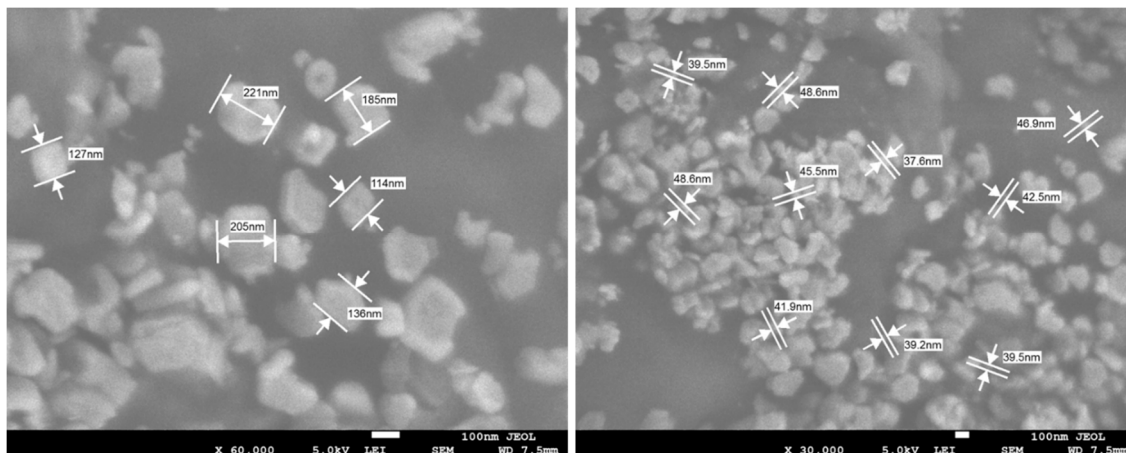


Figure 7. SEM image of gold nanoparticles (AuNPs) in the polymer matrix HLCuCl 0.05 wt% gold chloride 4 wt%, TEA 1wt%, and iodonium salt 1 wt% dissolved in EGDA 93.95 wt%.

All the hybrid nanocomposites with Au NPs formed in situ were explored by means of energy-dispersive spectroscopy (EDS), a technique that permits the quantification of the amount of material. In the EDS patterns (Figure 8), the characteristic peaks for C, O, N, Cl, I, and Cu along with the signal specific for elemental gold indicate that the reduction of gold ions to Au⁰ took place, thus supporting the results presented earlier. Hybrid nanocomposites with Au NPs formed in situ were explored by means of energy-dispersive spectroscopy (EDS), a technique that permits the quantification of the amount of material. In the EDS patterns (Figure 8), the characteristic peaks for C, O, N, Cl, I, and Cu along with the signal specific for elemental gold indicate that the reduction of gold ions to Au⁰ took place, thus supporting the results presented earlier.

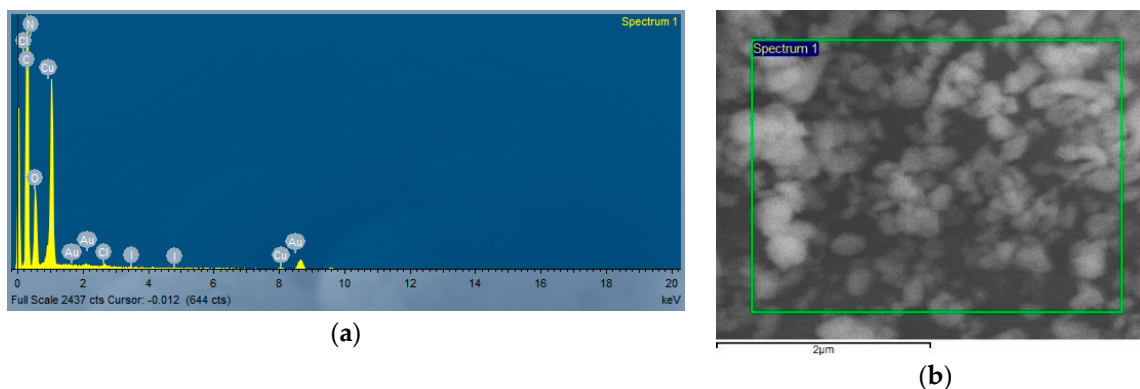


Figure 8. EDX graph of the polymer matrix (a), SEM image of the AuNPs in the polymer matrix (b).

4. Conclusions

In this paper, a new copper complex based on a hydrazone ligand was proposed as a photocatalyst for the polymerization of ethylene glycol diacrylate simultaneously with the production of gold nanoparticles in a polymer network under exposure to an LED at 419 nm. The short irradiation of the mixture containing copper complexes with polymerizable acrylate groups (EGDA) and H₂AuCl₄ in the presence of triethylamine and iodonium salt results in the formation of the desired composites with a good size of gold NPs (37–200 nm). The method described here is quite interesting because it allows

the simultaneous formation of gold nanoparticles and a lattice which secures the resulting structure and allows long-term stability. The morphology of the hardened systems, studied by SEM analysis, has shown that the nanoparticles are distributed homogeneously.

Supplementary Materials: The following are available online at <http://www.mdpi.com/2073-4360/12/10/2293/s1>: Figure S1: Mass spectrum of the ligand (HL). Figure S2: ¹H NMR spectrum of the ligand (HL). Figure S3: IR spectrum of the ligand (HL). Figure S4: IR spectrum of the copper complex. Figure S5. DTA, TGA and DrTGA of the ligand (HL). Figure S6: Cyclic voltammogram of HLCuCl in acetonitrile. Figure S7: Photoluminescence of HLCuCl in DMF. Figure S8. Evolution of the absorption spectra of irradiated mixtures ($\lambda_{\text{irr}} = 419 \text{ nm}$). Solution: HLCuCl 0.05 wt% and gold chloride 4wt% dissolved in 25 mL of DMF.

Author Contributions: Conceptualization, H.T., J.L.; formal analysis, H.T., N.K., T.I.K., J.L.; writing—original draft preparation, H.T., T.I.K., N.K., R.A., J.L.; data curation: H.T., T.I.K., N.K., R.A., J.L., B.G.; writing—review and editing, all authors. All authors have read and agreed to the published version of the manuscript.

Funding: This research was partly funded by Qassim University, represented by the Deanship of Scientific Research, on the material support for this research under the number (3847) during the academic year 2018.

Acknowledgments: The author gratefully acknowledges Qassim University, represented by the Deanship of Scientific Research, on the material support for this research under the number (3847) during the academic year 2018. Thanks are due to Fahad M. Alminderej for the fluorescence measurements.

Conflicts of Interest: The authors declare no conflict of interest.

References

1. Thomas, V.; Namdeo, M.; Murali, M.Y.; Bajpai, S.K.; Bajpai, M.J. Review on polymer, hydrogel and microgel metal nanocomposites: A facile nanotechnological approach. *Macromol. Sci. Pure App. Chem. A* **2008**, *45*, 107–119. [[CrossRef](#)]
2. Torrisi, V.; Ruffino, F. Metal-polymer nanocomposites: (Co-)evaporation/(Co)sputtering approaches and electrical properties. *Coatings* **2015**, *5*, 378–424. [[CrossRef](#)]
3. Thompson, R.B.; Ginzburg, V.V.; Matsen, M.W.; Balazs, A.C. Predicting the mesophases of copolymer-nanoparticle composites. *Science* **2001**, *292*, 2469–2472. [[CrossRef](#)] [[PubMed](#)]
4. Balazs, A.; Emrick, T.; Russel, T.P. Nanoparticle polymer composites: Where two small worlds meet. *Science* **2006**, *314*, 1107–1110. [[CrossRef](#)] [[PubMed](#)]
5. Boal, A.K.; Ilhan, F.; De Rouchey, J.E.; Thurn-Albrecht, T.; Russel, T.P.; Rotello, V.M. Self-assembly of nanoparticles into structured spherical and network aggregates. *Nature (London)* **2000**, *404*, 746–748. [[CrossRef](#)] [[PubMed](#)]
6. Balan, L.; Burget, D. Synthesis of metal/polymer nanocomposite by UV-radiation curing. *Eur. Polym. J.* **2006**, *42*, 3180–3189. [[CrossRef](#)]
7. Jose'-Yacama'n, M.; Perez, R.; Santiago, P.; Benaissa, M.; Gonsalves, K.; Carlson, G. Microscopic structure of gold particles in a metal polymer composite film. *Appl. Phys. Lett.* **1996**, *69*, 913–915. [[CrossRef](#)]
8. Stellacci, F.; Bauer, C.A.; Meyer-Friedrichsen, T.; Wenseleers, W.; Alain, V.; Kuebler, S.M.; Pond, S.J.K.; Zhang, Y.; Marder, S.R.; Perry, J.W. Laser and Electron-beam induced growth of nanoparticles for 2D and 3D metal patterning. *Adv. Mater.* **2002**, *14*, 194–198. [[CrossRef](#)]
9. Anyaogu, K.C.; Fedorov, A.V.; Neckers, D.C. Synthesis, characterization, and antifouling potential of functionalized copper nanoparticles. *Langmuir* **2008**, *24*, 4340–4346. [[CrossRef](#)]
10. Cioffi, N.; Torsi, L.; Ditaranto, N.; Tantillo, G.; Ghibelli, L.; Sabbatini, L.; Bleve-Zacheo, T.; D'Alessio, M.; Zambonin, P.G.; Traversa, E. Copper nanoparticle/polymer composites with antifungal and bacteriostatic properties. *Chem. Mater.* **2005**, *17*, 5255–5262. [[CrossRef](#)]
11. Sambhy, V.; MacBride, M.M.; Peterson, B.R.; Sen, A. Silver bromide nanoparticle/polymer composites: dual action tunable antimicrobial materials. *J. Am. Chem. Soc.* **2006**, *128*, 9798–9808. [[CrossRef](#)] [[PubMed](#)]
12. Scaiano, J.C.; Billone, P.; Gonzalez, C.M.; Maretti, L.; Marin, M.L.; McGilvray, K.L.; Yuan, N. Photochemical routes to silver and gold nanoparticles. *Pure Appl. Chem.* **2009**, *81*, 635–647. [[CrossRef](#)]
13. McGilvray, K.L.; Decan, M.R.; Wang, D.; Scaiano, J.C. facile photochemical synthesis of unprotected aqueous gold nanoparticles. *J. Am. Chem. Soc.* **2006**, *128*, 15980–15981. [[CrossRef](#)] [[PubMed](#)]

14. Marin, M.L.; McGilvray, K.L.; Scaiano, J.C. Photochemical Strategies for the Synthesis of Gold Nanoparticles from Au(III) and Au(I) Using Photoinduced Free Radical Generation. *J. Am. Chem. Soc.* **2008**, *130*, 16572–16584. [[CrossRef](#)]
15. Wang, D.Y.; Lin, H.C.; Yen, C.C. Influence of metal plasma ion implantation on photo-sensitivity of anatase TiO₂ thin films. *Thin Solid Films* **2006**, *515*, 1047–1052. [[CrossRef](#)]
16. Balan, L.; Malval, J.P.; Schneider, R.; Le Nouen, D.; Lougnot, D.J. In-situ fabrication of polyacrylate–silver nanocomposite through photoinduced tandem reactions involving eosin dye. *Polymer* **2010**, *51*, 1363–1369. [[CrossRef](#)]
17. Lu, Y.; Mei, Y.; Schrunner, M.; Ballauff, M.; Möller, M.W.; Breu, J. In situ formation of ag nanoparticles in spherical polyacrylic acid brushes by UV irradiation. *J. Phys. Chem. C* **2007**, *111*, 7676–7681. [[CrossRef](#)]
18. Balan, L.; Jin, M.; Malval, J.P.; Chaumeil, H.; Defoin, A.; Vidal, L. fabrication of silver nanoparticle-embedded polymer promoted by combined photochemical properties of a 2,7-diaminofluorene derivative dye. *Macromolecules* **2008**, *41*, 9359–9365. [[CrossRef](#)]
19. Balan, L.; Schneider, R.; Lougnot, D.J. A new and convenient route to polyacrylate/silver nanocomposites by light-induced cross-linking polymerization. *Prog. Org. Coat.* **2008**, *62*, 351–357. [[CrossRef](#)]
20. Balan, L.; Turck, C.; Soppera, O.; Vidal, L.; Lougnot, D.J. Holographic recording with polymer nanocomposites containing silver nanoparticles photogenerated in situ by the interference pattern. *Chem. Mater.* **2009**, *21*, 5711–5718. [[CrossRef](#)]
21. Sangermano, M.; Yagci, Y.; Rizza, G. In situ synthesis of silver–epoxy nanocomposites by photoinduced electron transfer and cationic polymerization processes. *Macromolecules* **2007**, *40*, 8827–8829. [[CrossRef](#)]
22. Çeper, T.; Arsu, N. Photochemically prepared gold/polymer nanocoatings: Formation of gold mirror. *Chem. Phys.* **2017**, *218*, 1700030. [[CrossRef](#)]
23. Anyaogu, K.C.; Cai, X.; Neckers, D.C. Gold nanoparticles photosensitized radical photopolymerization. *Photochem. Photobiol. Sci.* **2008**, *7*, 1469–1472. [[CrossRef](#)] [[PubMed](#)]
24. Yagci, Y.; Sangermano, M.; Rizza, G. In situ synthesis of gold-cross-linked poly(ethylene glycol) nanocomposites by photoinduced electron transfer and free radical polymerization processes. *Chem. Commun.* **2008**, 2771–2773. [[CrossRef](#)]
25. Lalevée, J.; Blanchard, N.; Tehfe, M.A.; Peter, M.; Morlet-Savary, F.; Fouassier, J.P. A novel photopolymerization initiating system based on an iridium complex photocatalyst. *Macromol. Rapid Commun.* **2011**, *32*, 917–920. [[CrossRef](#)]
26. Tehfe, M.A.; Lepeltier, M.; Dumur, F.; Gigmès, D.; Fouassier, J.P.; Lalevée, J. structural effects in the iridium complex series: Photoredox catalysis and photoinitiation of polymerization reactions under visible lights. *Macromol. Chem. Phys.* **2017**, *218*, 1700192. [[CrossRef](#)]
27. Tehfe, M.A.; Lalevée, J.; Telitel, S.; Sun, J.; Zhao, J.; Graff, B.; Morlet-Savary, F.; Fouassier, J.P. Iridium complexes incorporating coumarin moiety as catalyst photoinitiators: Towards household green LED bulb and halogen lamp irradiation. *Polymer* **2012**, *53*, 2803–2808. [[CrossRef](#)]
28. Tehfe, M.A.; Dumur, F.; Telitel, S.; Gigmès, D.; Contal, E.; Bertin, D.; Morlet-Savary, F.; Graff, B.; Fouassier, J.P.; Lalevée, J. Zinc-based metal complexes as new photocatalysts in polymerization initiating systems. *Eur. Polym. J.* **2013**, *49*, 1040–1049. [[CrossRef](#)]
29. Xiao, P.; Dumur, F.; Zhang, J.; Fouassier, J.P.; Gigmès, D.; Lalevée, J. Copper complexes in radical photoinitiating systems: Applications to free radical and cationic polymerization upon visible LEDs. *Macromolecules* **2014**, *47*, 3837–3844. [[CrossRef](#)]
30. Al Mousawi, A.; Kermagoret, A.; Versace, D.L.; Toufaily, J.; Hamieh, T.; Graff, B.; Dumur, F.; Gigmès, D.; Fouassier, J.P.; Lalevée, J. Copper photoredox catalysts for polymerization upon near UV or visible light: Structure/reactivity/efficiency relationships and use in LED projector 3D printing resins. *Polym. Chem.* **2017**, *8*, 568–580. [[CrossRef](#)]
31. Xiao, P.; Zhang, J.; Campolo, D.; Dumur, F.; Gigmès, D.; Fouassier, J.P.; Lalevée, J. Copper and iron complexes as visible-light-sensitive photoinitiators of polymerization. *J. Polym. Sci. Part A* **2015**, *53*, 2673–2684. [[CrossRef](#)]
32. Firmino, G.S.S.; De Souza, M.V.N.; Pessoa, C.; Lourenco, M.C.S.; Resende, J.A.L.C.; Lessa, J.A. Synthesis and evaluation of copper (II) complexes with isoniazid-derived hydrazones as anticancer and antitubercular agents. *BioMetals* **2016**, *29*, 953–963. [[CrossRef](#)] [[PubMed](#)]

33. Bergamini, F.R.G.; Nunes, J.H.B.; De Carvalho, M.A.; Ribeiro, M.A.; De Paiva, P.P.; Banzato, T.P.; Ruiz, A.L.T.G.; De Carvalho, J.E.; Lustrì, W.R.; Martins, D.O.T.A.; et al. Polynuclear copper(II) complexes with nalidixic acid hydrazones: Antiproliferative activity and selectivity assessment over a panel of tumor cells. *Inorganica Chim. Acta* **2019**, *484*, 491–502. [[CrossRef](#)]
34. Rocha, C.S.; Filho, L.F.O.B.; De Souza, A.E.; Diniz, R.; Denadai, Â.M.L.; Beraldo, H.; Teixeira, L.R. Structural studies and investigation on the antifungal activity of silver(I) complexes with 5-nitrofurán-derived hydrazones. *Polyhedron* **2019**, *170*, 723–730. [[CrossRef](#)]
35. Bakale, R.P.; Naik, G.N.; Machakanur, S.S.; Mangannavar, C.V.; Muchchandi, I.S.; Gudasi, K.B. Structural characterization and antimicrobial activities of transition metal complexes of a hydrazone ligand. *J. Mol. Struct.* **2018**, *1154*, 92–99. [[CrossRef](#)]
36. Ramachandran, E.; Gandin, V.; Bertani, R.; Sgarbossa, P.; Natarajan, K.; Bhuvanesh, N.S.P.; Venzo, A.; Zoleo, A.; Glisenti, A.; Dolmella, A.; et al. Synthesis, characterization and cytotoxic activity of novel copper (II) complexes with aroylhydrazone derivatives of 2-Oxo-1,2-dihydrobenzo[h]quinoline-3-carbaldehyde. *J. Inorg. Biochem.* **2018**, *182*, 18–28. [[CrossRef](#)]
37. Rehm, D.; Weller, A. Kinetics of fluorescence quenching by electron and h-atom transfer. *Isr. J. Chem.* **1970**, *8*, 259–271. [[CrossRef](#)]
38. Manivannan, S.; Dhanuskodi, S. Synthesis, crystal growth, structural and optical properties of an organic NLO material. *J. Cryst. Growth* **2004**, *262*, 473–478. [[CrossRef](#)]
39. Kashar, T.I. Synthesis, characterization, biological and anticancer activity of new Pd (II), Pt (IV), V (III) and Ru (III) complexes with a schiff base ligand deriving from dehydroacetic acid. *J. Chem. Pharm. Res.* **2017**, *9*, 164–173.
40. AbouEl-Enein, S.; El-Saied, F.A.; Emam, S.M.; Ell-Salamony, M.A. First row transition metal complexes of salicylidene and 2-hydroxy-1-naphthylidene-N-cyanoacetohydrazone. *Spectrochim. Acta Part A* **2008**, *71*, 421–429. [[CrossRef](#)]
41. Phaniband, M.A.; Dhumwad, S.D.; Pattan, S.R. Synthesis, characterization, antimicrobial, and DNA cleavage studies of metal complexes of coumarin Schiff bases. *Med. Chem. Res.* **2011**, *20*, 493–502. [[CrossRef](#)]
42. Nakamoto, K. Infrared and raman spectra of inorganic and coordination compounds. *Appl. Organomet. Chem.* **1999**, *13*, 857–858.
43. Deng, J.; Chen, W.; Deng, H. Synthesis of DipyrídyI Ketone Isonicotinoyl Hydrazone Copper(II) Complex: Structure, Anticancer Activity and Anticancer Mechanism. *J. Fluoresc.* **2016**, *26*, 1987–1996. [[CrossRef](#)] [[PubMed](#)]
44. Chew, S.T.; Lo, K.M.; Lee, S.K.; Heng, M.P.; Teoh, W.Y.; Sim, K.S.; Tan, K.W. Copper complexes with phosphonium containing hydrazone ligand: Topoisomerase inhibition and cytotoxicity study. *Eur. J. Med. Chem.* **2014**, *76*, 397–407. [[CrossRef](#)]
45. Vafazadeh, R.; Moghadas, Z.; Willis, A.C. Anion and solvent effects on the coordination behavior of N-(2-pyridinylmethylene)benzoylhydrazone with copper(II): Synthesis and structural characterization. *J. Coord. Chem.* **2015**, *68*, 4255–4271. [[CrossRef](#)]
46. Wong, K.M.-C.; Hung, L.-L.; Lam, W.H.; Zhu, N.; Yam, V.W.-W. A class of luminescent cyclometalated alkynylgold(III) complexes: Synthesis, characterization, and electrochemical, photophysical, and computational studies of [Au(C[^]N[^]ΛC)(CtCsR)] (C[^]N[^]ΛC) K₃C,N,C Bis-cyclometalated 2,6-Diphenylpyridyl). *J. Am. Chem. Soc.* **2007**, *129*, 4350–4365. [[CrossRef](#)]
47. Kumar, D.; Syamal, A.; Gupta, P.K. Coordination compounds of polystyrene-supported azo dye. *J. Indian Chem. Soc.* **2007**, *84*, 217–222.
48. Osman, A.H. Synthesis and characterization of cobalt (II) and nickel (II) complexes of some Schiff bases derived from 3-hydrazino-6-methyl [1,2,4] triazin-5(4H) one. *Transit. Met. Chem.* **2006**, *31*, 35–41. [[CrossRef](#)]
49. Bharti, S.K.; Patel, S.K.; Nath, G.; Tilak, R.; Singh, S.K. Synthesis, characterization, DNA cleavage and in vitro antimicrobial activities of copper (II) complexes of Schiff bases containing a 2,4-disubstituted thiazole. *Transit. Met. Chem.* **2010**, *35*, 917–925. [[CrossRef](#)]
50. Lalevée, J.; Dumur, F.; Mayer, C.R.; Gígmes, D.; Nasr, G.; Tehfe, M.A.; Telitel, S.; Morlet-Savary, F.; Graff, B.; Fouassier, J.P. Photopolymerization of N-Vinylcarbazole using visible-light harvesting iridium complexes as photoinitiators. *Macromolecules* **2012**, *45*, 4134–4141. [[CrossRef](#)]
51. Newman, J.D.S.; Blanchard, G.J. Formation of gold nanoparticles using amine reducing agents. *Langmuir* **2006**, *22*, 5882–5887. [[CrossRef](#)] [[PubMed](#)]

52. Bindhu, M.R.; Parimaladevi, R.; Umadevi, M. Monodispersed gold nanoparticles as a probe for the detection of Hg^{2+} ions in water. *Acta Chim. Slov.* **2017**, *64*, 186–192.
53. Ghosh, P.; Chattopadhyay, N. Gold nanoparticles: Acceptors for efficient energy transfer from the photoexcited fluorophores. *Opt. Photonics J.* **2013**, *3*, 18–26. [[CrossRef](#)]
54. Tsuji, M.; Hashimoto, M.; Nishizawa, Y.; Tsujiy, T. Preparation of gold nanoplates by a microwave-polyol method. *Chem. Lett.* **2003**, *32*, 1114–1115. [[CrossRef](#)]
55. Alsawafta, M.; Badilescu, S.; Paneri, A.; Truong, V.V.; Packirisamy, M. Gold-Poly(methyl methacrylate) nanocomposite films for plasmonic biosensing applications. *Polymers* **2011**, *3*, 1833–1848. [[CrossRef](#)]
56. Lin, J.T.; Liu, H.W.; Chen, K.T.; Cheng, D.C. Modeling the optimal conditions for improved efficacy and crosslink depth of photo-initiated polymerization. *Polymers* **2019**, *11*, 217. [[CrossRef](#)]
57. Abdallah, M.; Hijazi, A.; Lin, J.-T.; Graff, B.; Dumur, F.; Lalevée, J. Coumarin derivatives as photoinitiators in photo-oxidation and photo-reduction processes and a kinetic model for simulations of the associated polymerization profiles. *App. Polym. Mater.* **2020**, *2*, 2769–2780. [[CrossRef](#)]



© 2020 by the authors. Licensee MDPI, Basel, Switzerland. This article is an open access article distributed under the terms and conditions of the Creative Commons Attribution (CC BY) license (<http://creativecommons.org/licenses/by/4.0/>).